PERGAMON

International Journal of Heat and Mass Transfer 44 (2001) 2711–2726

International Journal of HEAT and MASS TRANSFER

www.elsevier.com/locate/ijhmt

Effect of slot gas injection to the flow field and coherent structure characteristics of a backstep flow

Harinaldi *, Toshihisa Ueda, Masahiko Mizomoto

Department of Mechanical Engineering, Graduate School of Science and Technology, Keio University, 3-14-1 Hiyoshi, Kohoku-ku, Yokohama 223-8522, Japan

Received 8 January 2000; received in revised form 7 September 2000

Abstract

The flow field and coherent structure of the flow over a backstep with slot-gas-injection were investigated. The mean flow, turbulence properties and coherent structure characteristics are significantly influenced by the increase of injection momentum near the step (l_f/H = 2). The mean flow field is characterized by recirculation zone splitting, with mass transfer of injected gas toward each part depending on the specific momentum ratio of injection. More mass entrainment, turbulence structures alteration in the shear layer and the hydrodynamic disturbances from the injection flow suppress the coherent structure velocity, size and detachment. These results provide basis information for achieving the balance of competing factors between geometrical and fluid dynamical parameters of injection to establish an efficient design of a combustor from the perspective of enhancing the gas–air mixing process.

1. Introduction

A fluid flow characterized as having flow separation adjacent to a solid boundary, such as the one over a backward facing step, has applications in a wide range of engineering practices. One practical interest that gives primary motivation of this study involves its utilization in the combustion area. In this regard, injecting a fuel to a low-speed recirculating airflow behind the step to produce a diffusion flame is a common method in a flame holder of many combustor configurations that even operate in a high-speed flow. However, this diffusion flame is inherently large more complex than a simple jet since its structure and characteristics vary to a large extent, depending on the method and character of the arrangement of air inlet, the introduction of the fuel, the geometry of the containment as well as the flow field structures involved. The key feature embedded in those affecting factors is the mixing process between the injected fuel and the surrounding air that is controlled by convective mass transfer and diffusion mechanism, which has not yet been well characterized at a fundamental level so that the practical applications have to rely heavily on the empirical information.

From a literature search, it appears that most of the published works of the backstep-flow deal with the case of no mass addition [1–3]. Only limited studies have addressed the issue of mass injection to the recirculation zone of the backstep-flow. Among them, de Groot et al. [4,5] used a Rayleigh measurement and later combined it with an LDV to determine the bleed CO_2 gas concentration and the velocity distribution to simulate turbulent mass transport of gas emanating from a solid fuel of a solid-fueled ramjet. Intensive studies on a backstep-flow with mass addition from porous plate in non-reactive flow field had been done by Yang's group which included experimental measurement on velocity field [6], and high-temperature heat transfer [7]. A numerical study on the similar flow condition was made by Yang and Kuo [8]. Both experimental and numerical results showed that mass addition changed the mean velocity, the turbulence features and the heat transfer characteristic of the flow field. In the case of flow field with combustion, Haibel and Mayinger [9] investigated the effect of injection angle and injection geometry to the

* Corresponding author. Tel.: +81-045-563-1141; fax.: +81-045-563-5943.

E-mail address: d976204@msr.st.keio.ac.jp (Harinaldi).

0017-9310/01/$ - see front matter
PII: S0017-9310(00)00301-X

Nomenclature

f_{dc}	detaching frequency of the coherent structure
H	step height
h_{cs}	coherent structure height
I	specific momentum ratio of injection, $\rho_{N2}V_{N2}^2/\rho_o U_o^2$
K	shear correlation coefficient, $-\overline{uv}/(\sqrt{\overline{u^2}}\sqrt{\overline{v^2}})$
l_f	horizontal distance from the step to the injection port
Re_H	Reynolds number based on step height, $U_o H/v_o$
TI	turbulence intensity
U, u	streamwise instantaneous velocity and velocity fluctuation
U_{cv}	convection velocity of coherent structure
$-\overline{uv}$	Reynolds shear stress
V, v	cross-stream instantaneous velocity and velocity fluctuation
$W_{1/2}$	half of test section width
x	horizontal distance from the step
x_{cs}	horizontal distance from the step to vortex structure in the coherent structure
y	vertical distance from the base wall
z	spanwise distance from the center of the channel

Greek symbols

ρ	density
v	kinematics viscosity
ω	vorticity
ψ	stream function

Subscripts

o	inlet air freestream
N2	nitrogen gas jet injection

cold and reactive mixing of gas injected upstream of a step and they proposed a prediction of the mixing jet development. More recently, Coats and his associates [10] studied the interaction between the combustion process and the coherent structures in a diffusion flame behind a backward facing step. They mentioned some important characters of interaction between the coherence structuring and the combustion process. However, in the aforementioned studies, detailed information of how the structures and the dynamic behaviors of recirculation zone and the mixing layer in the shear region will respond to the mass addition has not been completely cleared. Thus, there rises a need to clarify that interaction, even still at the stage of the absence of chemical reaction.

In a typical application initially mentioned, special attentions must be placed on the recirculation zone, which consists of a mixing layer in the shear region and a reverse flow, since it is an essential feature in all high-intensity combustion systems [10]. Besides, a two-dimensional gas injection from the slot port to the recirculation zone serving as a means of fuel feeding in a practical combustion system, may be regarded as the forcing agent to the mixing layer of interest which usually contains large-scale three-dimensional features. With the imposition of this forcing, the crucial role of these three-dimensional large scales to the dynamics of the mixing layer will undergo some modifications, giving direct effects to the flow of energy to the small scales, the rate of fluid mixing at the molecular scale, and the associated rates of strain experienced by the fluid or by the element of flame, if it involves a combusting flows. Hence, any inherent tendency towards the alteration of the structure and behavior of recirculating flow is therefore of considerable interest to be comprehensively examined. To address the above issues, the present work was undertaken with the objective to gain comprehensive quantitative and qualitative information on the subject through a detailed measurement of the turbulence structure and visualization of the flow field. Although the experimentation was done in an isothermal flow without involving any chemical reaction, the results were targeted to contribute an underlying knowledge of the hydrodynamics aspects of the mechanism and turbulence influence in gas–air mixing process. Furthermore, this work also includes the examination of the coherent structures since, as an integral part of the flow field, the coherent structures can have profound effects on local patterns of mixing and strain and thus the whole character of the combustion process in the practical system.

2. Experiments

2.1. Apparatus and instrumentation

A schematic diagram of the apparatus and instrumentation is shown in Fig. 1. The air was driven by a vortex blower into a horizontal small-scale wind tunnel after first passing through an orifice manometer system to maintain a constant flow rate over extensive period. The main air then flowed through an arrangement of a diffuser, a settling chamber, a straightener, three screens, a converging nozzle and a test section. The cross-section of the test section upstream of the step was 50×80 mm^2. The step height H was 20 mm and the length of the test section was 300 mm. In the base wall, a gas injection port with 1 mm-slot exit spanned across the test section was installed at a distance l_f from the step, and through it nitrogen gas was injected upward into the test section. The coordinate system was set as in Fig. 1.

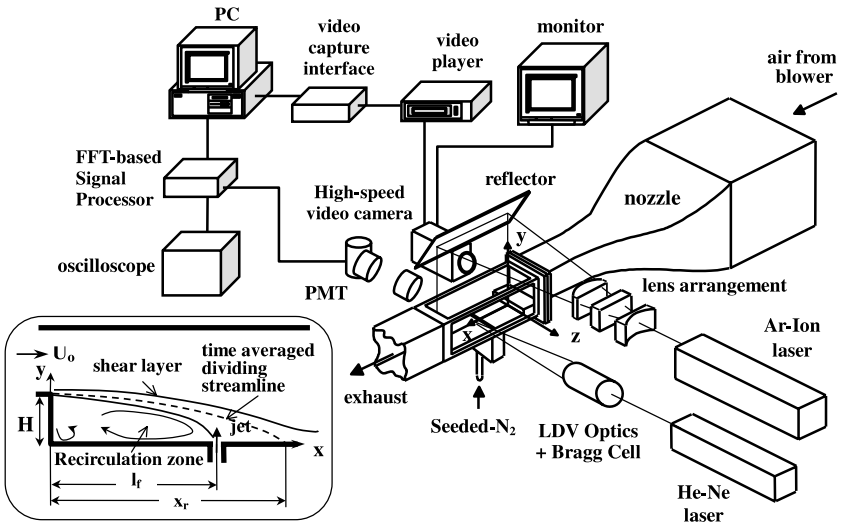

Fig. 1. Schematic diagram of the experimental apparatus and instrumentation.

Instantaneous velocity was measured by a 15 mW forward-scattered dual beam He–Ne LDV system with a Bragg cell to detect flow reversal. The details of the LDV system, the measured velocity components, the method of deriving velocity cross-correlation, data reduction, and estimation of statistical uncertainty have been described in our previous paper [11]. Laser sheet-based flow visualization was conducted with a 4 W – 514.5 nm Argon-ion laser (Coherent Innova 70-4) with cylindrical lens arrangement and a high-speed video camera (Motion Scope HR Series). A 0.4 mm-thickness and 100 mm-width laser sheet was made in the plane of visualization. The high-speed video camera was set to capture 1000 frames/s and the shutter speed was 1/2000 s. The recording time was about 2 s that yields a video movie of 2048 frames for each parameter condition. The image recording was done in a dark room condition to suppress the background light. The recorded video movies were then transmitted to a personal computer for further direct image analysis on the frame-by-frame basis. For analyzing the video images, software was developed to do geometrical measurement and to recognize the luminance intensity on the image. Particle seeding system for both LDV or laser sheet visualization was similar to that of Ueda et al. [12]. In velocity measurement, the particles were seeded directly to the main air flow, meanwhile for visualization, the particles were seeded to the injected gas supply system.

2.2. Test condition

Over the entire experiments of the present study, the upstream main airflow velocity was maintained constant at $U_o = 10$ m/s. The Reynolds number based on this velocity and step height ($Re_H = U_o H/v_o$) was 1.25×10^4. The initial velocity measured at position $x = -2$ mm (upstream of the step edge) showed a distribution of a uniform flow with turbulent intensity of about 0.7%. The maximum turbulent intensity in the boundary layer was about 3%, and the thickness of boundary layer before the separation is about 3 mm ($\delta/H = 0.15$). The distance from the step to the reattachment point defined as the location with zero mean streamwise velocity at 0.05 H above the base wall was 5.5 H. In the experiments, the principal parameters were the ratio of specific momentum between the injected nitrogen and the main airflow ($I = \rho_{N2} V_{N2}^2/\rho_o U_o^2$) and the streamwise distance from the step to the injection slot (l_f). The specific momentum ratio of injection was varied from 0 to 0.3 by altering the nitrogen injection velocity, keeping the airflow velocity U_o ($=10$ m/s). Two cases of gas injection location within the recirculation zone, where the flow condition was different, were selected. In case (a), the injection was at near step position ($l_f/H = 2$) where the region was dominated by recirculating flow, while in case (b), it was at near reattachment position ($l_f/H = 4$), where the shear turbulence was predominant (see inset in Fig. 1).

In order to get a comprehensive insight of the velocity field, the velocity was measured at a number of selected stations with the main measurements at center vertical plane located around the injection point. Summary of the measurement parameters and stations can be seen in Table 1. Meanwhile, the flow visualization of the image of the coherence structure formation was conducted at vertical center plane, focussed on the shear layer region.

Table 1
Velocity measurement station

Injection location (mm)	Specific momentum ratio of injection	Measurement station		
		x (mm)	y (mm)	z (mm)
$l_f = 40$	$I = 0, 0.01, 0.04, 0.1, 0.3$	15–65	2–40	0
	$I = 0.04, 0.3$	40	10, 18, 34	−38 to 38
$l_f = 80$	$I = 0, 0.01, 0.04, 0.1, 0.3$	55–105	2–40	0
	$I = 0.04, 0.3$	80	10, 18, 34	−38 to 38

3. Results and discussion

3.1. Mean characteristics of the flow field

3.1.1. Mean velocity profiles

The characteristics of mean streamwise and cross-stream velocity profiles at several measurement stations around the injection point have been compared for the two cases of injection location in our previous report [11]. The results showed that the effect of increasing the specific momentum ratio of injections to the mean velocity profiles was more remarkable as the gas was injected at near step position ($l_f/H = 2$) compared to the case of injection at near reattachment region ($l_f/H = 4$). The variation of the mean velocity occurred as a response to balance the creation of mass increase due to gas addition to satisfy the momentum conservation. For brevity, a portion of the streamwise velocity profiles near the injection location is redisplayed in Fig. 2(a), and the data of Yang et al. [6] are also included for comparison. The injection velocity in Yang's work was much lower compared to the present work. Thus, their profiles quite agree only to the case of $I = 0$ of the present results. Meanwhile, Fig. 2(b) displays the spanwise distribution of mean streamwise velocity above the injection point ($x/H = l_f/H = 2$) for three different heights, each representing different flow region, i.e., free stream region at $y/H = 1.7$, shear layer region at $y/H = 0.9$ and recirculation zone at $y/H = 0.5$. Fig. 2(b) is presented only at half of span width due to the symmetric distribution. The velocity profiles for $I = 0.3$ maintain their uniformity up to 85% of spanwise region at $y/H = 1.7$ and 0.9, and up to 75% at $y/H = 0.5$. Beyond this region, the sidewall effect comes into account. Meanwhile, for the case of $I = 0.04$, only at $y/H = 1.7$, which is located at the freestream, the uniformity of velocity distribution along the spanwise direction is quite well (up to 85%). At the shear layer region and recirculation zone, the velocity deviates from the center plane value to a lower forward velocity and to a higher reverse velocity, respectively. The deviations reach maximum just before the location where the wall effect becomes prominent. This comparison suggests the enhancement of the two-dimensionality of the flow field by increasing the specific momentum ratio of injection. Closing further to the sidewall, the profiles in the recirculation region ($y/H = 0.5$) suggest another significant feature. The velocity distributions for both cases of specific momentum ratio show that the reverse flows decrease, vanish and then switch to be forward flows. The profiles suggest that there formed a secondary spanwise-oriented recirculating flow in the near sidewall region. As far as to the authors' knowledge, the experimental work mentioned some spanwise profiles only that of Armaly et al. [13]. Despite the difference in the flow condition, their trend of profiles at the corresponding vertical position to the present result is in a qualitative agreement, such as described in Fig. 2(b). However, it is difficult to make a conclusive interpretation about the near sidewall structure from both experimental findings because of limited data. Indeed, the spanwise-oriented recirculating flow near the sidewall is possible to represent only the x–z plane projection of a more complex three-dimensional separation region that exists along the sidewall corner. Only until recently some numerical studies [14,15] have predicted three-dimensional structure near the side wall in detail which suggests that the transition from two- to three-dimensional flow is a result of a continuous penetration of three-dimensional flow, fed by a wall jet, from the sidewall to the central plane. However, the limitation of these predictions to the case of laminar flow suggests that more intensive studies in the future are needed to address this issue. In case of injection at $l_f/H = 4$, spanwise distributions indicate similar trends regarding the effect of increasing the specific momentum to the enhancement of the uniformity of the velocity profiles and the trends of the profiles near the sidewall.

3.1.2. Mean streamlines

To highlight the flow field variation especially in the portion of flow region exhibiting two-dimensionality (which covers no less than 75% of the flow field), the mean streamlines, pattern at the center plane of the flow field, are constructed from the measured mean velocity data. The stream function (ψ) is defined as

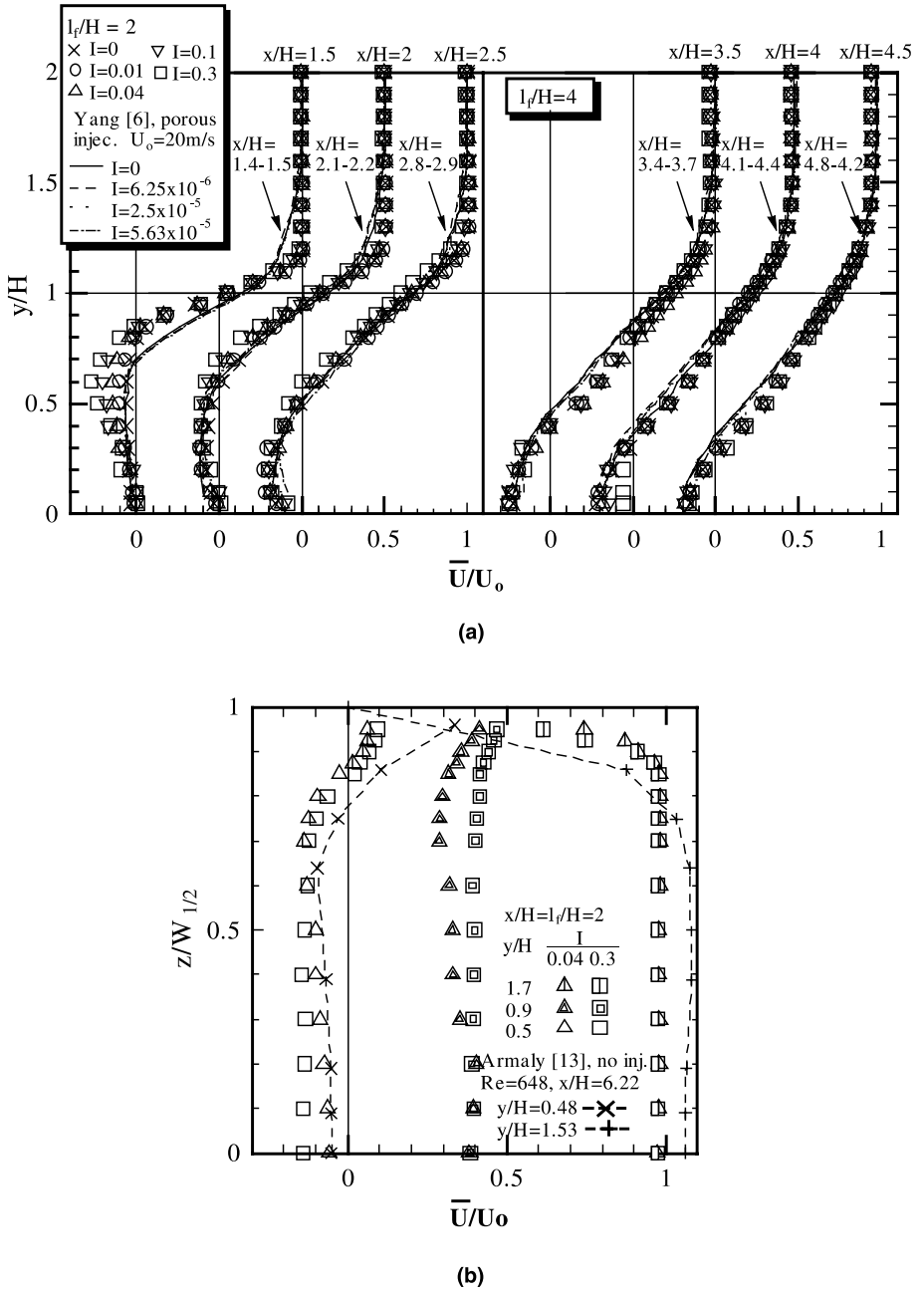

Fig. 2. Several profiles of mean streamwise velocity, center plane distribution in case of: (a) $l_f/H = 2$; (b) $l_f/H = 4$; (c) spanwise distribution, $l_f/H = 2$.

$$d\psi = \frac{\partial \psi}{\partial x}\,dx + \frac{\partial \psi}{\partial y}\,dy, \tag{1}$$

where

$$U = \frac{\partial \psi}{\partial y} \tag{2a}$$

and

$$V = -\frac{\partial \psi}{\partial x}. \tag{2b}$$

Therefore, the mean mass flow rate, which equals to the difference between two stream functions, is determined

from the following equations (with over bar to present mean value):

$$\int_1^2 \mathrm{d}\overline{\psi} = -\int_{x1}^{x2} \overline{V}\,\mathrm{d}x + \int_{y2}^{y1} \overline{U}\,\mathrm{d}y \approx -\sum_1^2 \overline{V}\,\mathrm{d}x + \sum_1^2 \overline{U}\,\mathrm{d}y. \quad (3)$$

The calculated result is then presented in the form of lines of constant $\overline{\psi}/(U_o H)$.

Figs. 3(a)–(e) show the evolution of the mean streamlines due to the gas injection. When no gas is injected (Fig. 3(a)), the maximum mass flow rate in the reverse flow region corresponds to a value of $\overline{\psi}/(U_o\mathrm{H})$ about -0.06. This is a typical value for a recirculating flow over backstep without mass addition [2,6]. The pattern also indicates that the remarkable recirculation flow extents to an area between $x/H = 1$ to reattachment point, $x/H = 5.5$. Although not stagnant, the flow in region between $x/H = 0$ and $x/H = 1$ has reverse velocity near zero, thereby the streamlines are beyond the range of interest and not drawn. Injecting the gas in the near step location ($l_f/H = 2$) significantly alters the mean streamlines pattern of the recirculation region. At $I = 0.04$ (Fig. 3(b)), the streamlines pattern shows that there formed two recirculating flow pattern, upstream and downstream of injection location. The gas injection gives the blocking effect to the recirculation zone that makes it split into two. The non-dimensional mass flow rates $\overline{\psi}/(U_o H)$ in both recirculation zones show not to much different value about -0.07, which is a little increase from the case of no mass addition. The quite similar value of $\overline{\psi}/(U_o\mathrm{H})$ in both recirculation zones suggests that the mass transfer from this low-momentum injected gas occur equally toward upstream and downstream directions from the injection point. On the other hand, when the gas is injected with $I = 0.3$, Fig. 3(c) shows that recirculating mass flow rate has a value of $\overline{\psi}/(U_o\mathrm{H})$ about -0.14 in the upstream recirculation flow and about -0.08 in the downstream one. The increase of mass flow rate in the upstream recirculation zone is about four times to that in the downstream one. The bulk flow of the injected gas with high momentum tends to convect mostly toward the upstream location which is initially a quieter region that gives less flow restriction. In every case of injection discussed above, the total amount of mass flow rate increase in both recirculation zones is quite equal to the mass flow rate addition from the gas injection, which suggests that all the injected gas are engulfed in the recirculation zones without penetrating through the shear layer region into the freestream. Furthermore, it is clear that as injection momentum is increased, an enlargement of the area containing recirculation flow takes places, indicating by the sifting of the dividing streamline ($\overline{\psi}/(U_o H) = 0$) to higher vertical position as much as about 16% in the case of $I = 0.3$. We suggest that as ratio of injection momentum is increased, the vertical penetration effect of the injected gas becomes more significant in the recirculation zone. There should be an increase in the static pressure in the recirculation zone, which makes a decrease in pressure difference across the shear layer. Consequently, the size of recirculation zone increases.

While the gas is injected at $l_f/H = 4$, Fig. 3(d) shows that in the case of $I = 0.04$, there is no significant difference of the streamlines pattern compared to the case of no injection. The mass flow rate in the recirculation zone slightly increases due to the mass addition. When the injection momentum is increased to $I = 0.3$, it can be figured out from Fig. 3(e) that the gas injection creates another recirculation zone downstream of the injection point. The mass flow rate in the original upstream recirculation zone increases only slightly, which indicates that the injected mass mainly distributes toward the downstream recirculation zone, created by the injection. However, the total mass flow rate increase at the upstream recirculation zone and the mass flow rate that enters the downstream one is less than the mass flow rate supplied by the injection. This result suggests that the injected gas penetrates deeply through the recirculation zone and part of it is carried out by the freestream.

3.1.3. Mean vorticity

The mean vorticity distributions are constructed from the measured mean velocity data. The mean vorticity is calculated as follows:

$$\overline{\omega} = \frac{1}{2}\left[\left(\frac{\partial \overline{V}}{\partial x}\right) - \left(\frac{\partial \overline{U}}{\partial y}\right)\right]. \quad (4)$$

In the above equation, the mean velocity gradient has been determined from the following approximation (presented here only the streamwise velocity gradient).

$$\left(\frac{\partial \overline{U}}{\partial y}\right)_i = \frac{1}{2}\left(\frac{\overline{U}_{i+1} - \overline{U}_i}{y_{i+1} - y_i} + \frac{\overline{U}_i - \overline{U}_{i-1}}{y_i - y_{i-1}}\right), \quad (5)$$

where the subscript $i-1$, i, and $i+1$ denote consecutive measurement points. The calculation result is then presented in the form of lines of constant $(\overline{\omega}H)/U_o$ as shown in Figs. 4(a)–(e).

Fig. 4(a) suggests that in case of no gas injection, the flow field is dominated by negative (clockwise) vorticity in the shear layer and most part of recirculation zone. The region of concentrated high-negative vorticity is initiated at the edge of the step and further downstream the negative vorticity weakens. The absolute value of vorticity is higher in the shear layer region compared to that in the recirculation zone because of higher mean velocity gradient in the shear layer region. Later in the discussion of coherence structure, we will show in our tomographic images that this region is

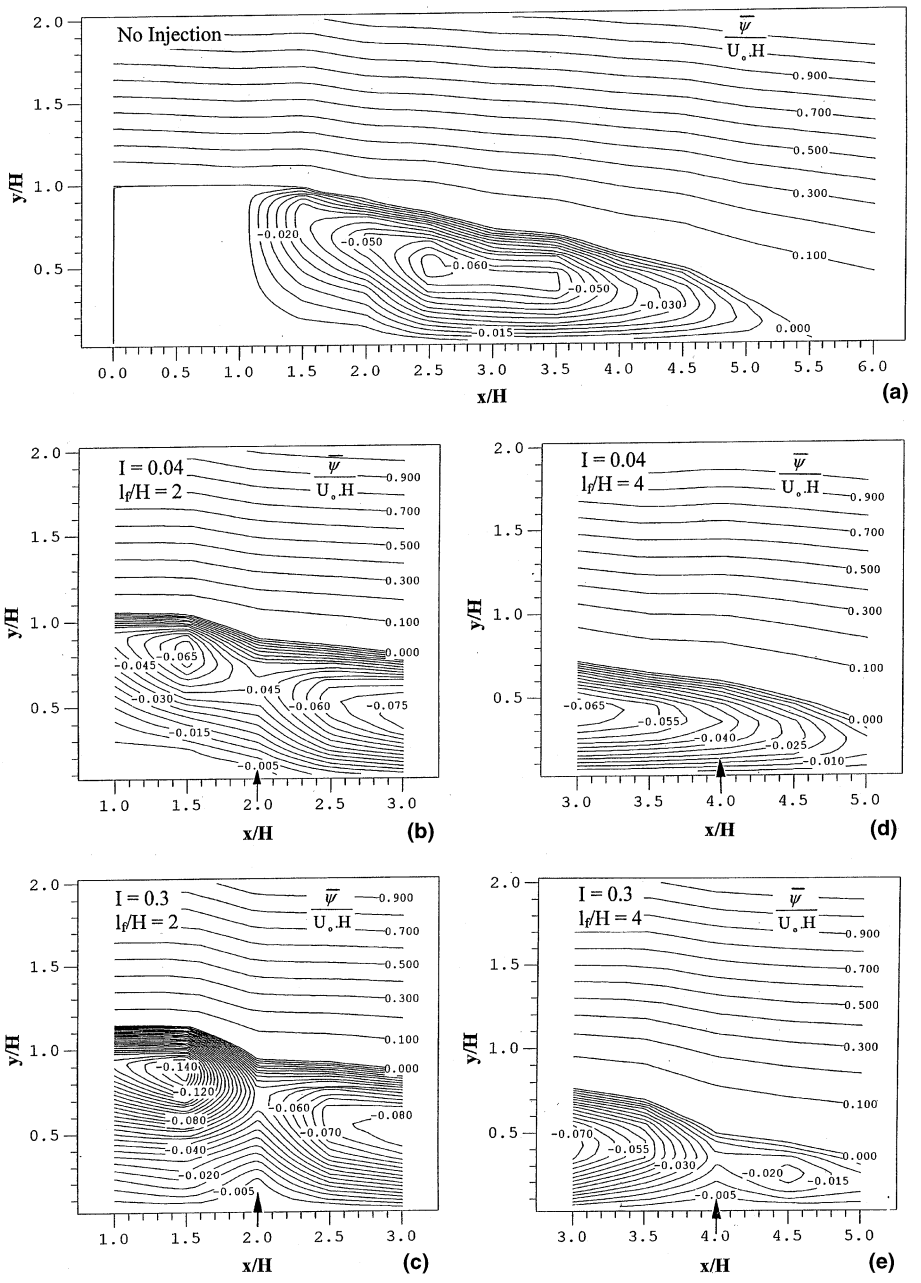

Fig. 3. Effects of the gas injections to the variations of mean streamline patterns: (a) no injection, $I = 0$; (b) $l_f/H = 2$, $I = 0.04$; (c) $l_f/H = 2$, $I = 0.3$; (d) $l_f/H = 4$, $I = 0.04$; (e) $l_f/H = 4$, $I = 0.3$ (contour interval is 0.1 for $\overline{\psi} > 0$ and 0.005 for $\overline{\psi} < 0$).

dominated by the swirling structures which are convected downstream with velocity approximately a half of main freestream velocity. When the gas is injected to the flow field at $l_f/H = 2$, Figs. 4(b) and (c) show that there is induced in the upstream from the injection point, a region which has positive (counter clockwise) mean vorticity. As the specific momentum ratio increases from $I = 0.04$ to 0.3, the region becomes larger and the mean positive vorticity increases up to a maximum value of $(\overline{\omega}H)/U_o$ about 0.5. This suggests that the injection creates vortices which rotate in an opposite angular direction to those induced at the shear layer region. The accumulation of vorticity production towards the upstream region brings about most fraction of the injected gas distributes to the region. Furthermore, increasing the specific momentum ratio

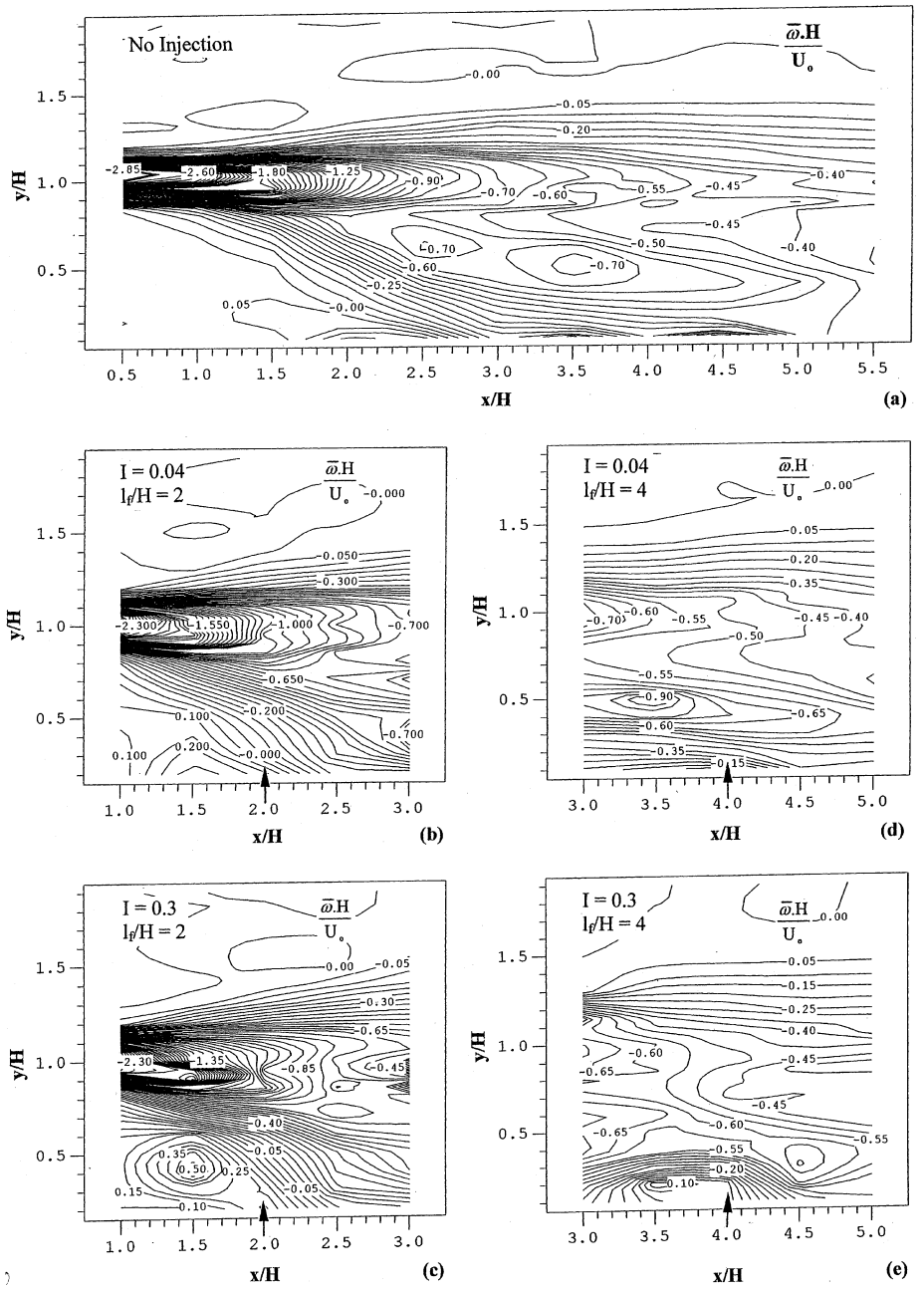

Fig. 4. Effects of the gas injections to the variations of mean vorticity patterns: (a) no injection, $I = 0$; (b) $l_f/H = 2$, $I = 0.04$; (c) $l_f/H = 2$, $I = 0.3$; (d) $l_f/H = 4$, $I = 0.04$; (e) $l_f/H = 4$, $I = 0.3$ (contour interval is 0.05).

of injection gives remarkable influence to the vorticity dissipation rate in the shear layer region as one can see that the attenuation of mean vorticity as it convected downstream occurs sooner. Meanwhile, in case of the gas which is injected at $l_f/H = 4$ in Figs. 4(d) and (e), the mass injection gives no remarkable effects to the mean vorticity field. In most part of the flow field, the vorticity is negative. Even with the highest ratio of specific momentum injection in the experiment ($I = 0.3$), a weak positive vorticity with maximum value of $(\overline{\omega}H)/U_o$ about 0.1 occupies only a small portion of region near the injection point. Moreover, there is no indication that the dissipation of vorticity in the shear layer region is effected by the gas injection. This confirms the domination of high-shear turbulence in the reattachment region.

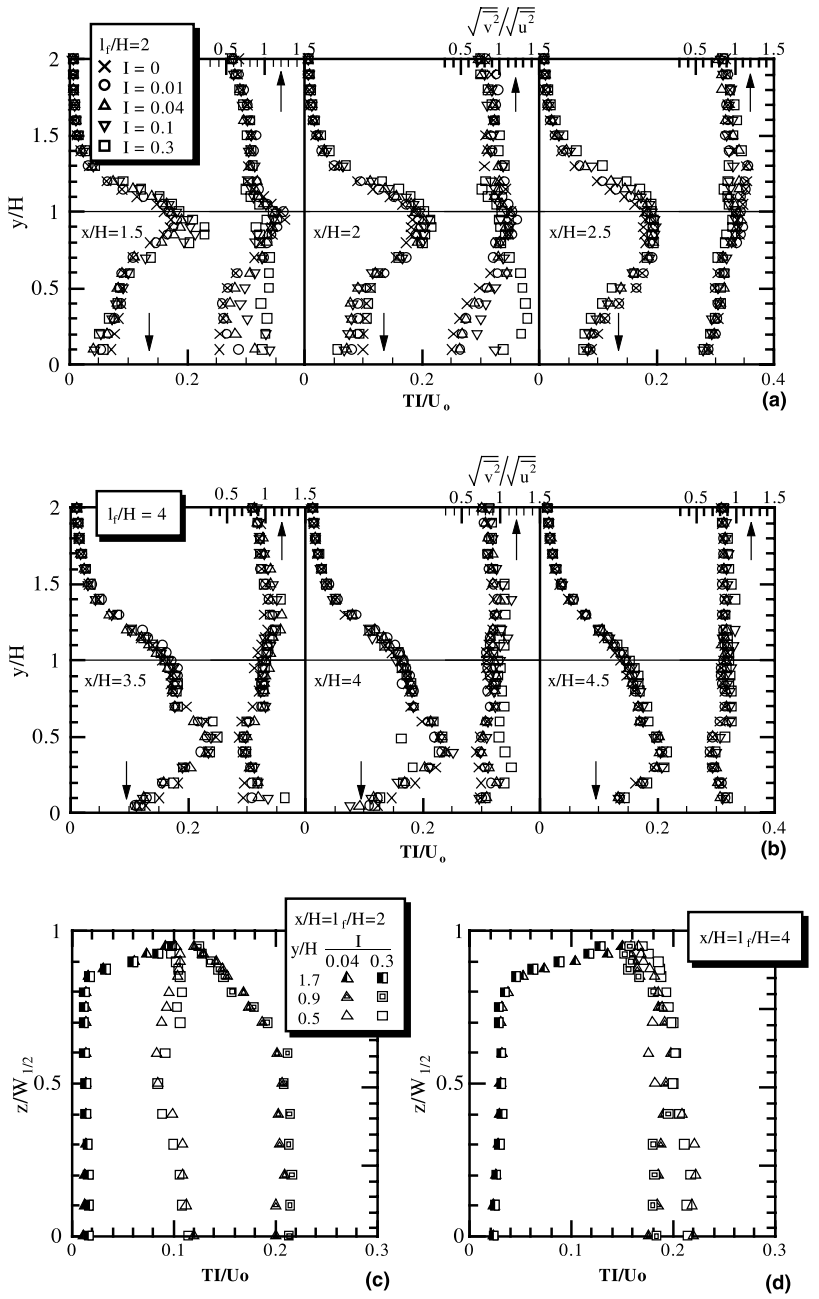

Fig. 5. Profiles of turbulence intensity and ratio of rms of fluctuating velocities. Center plane distribution in case of: (a) $l_f/H = 2$; (b) $l_f/H = 4$, and spanwise distribution above the injection in case of (c) $l_f/H = 2$; (d) $l_f/H = 4$.

3.2. Turbulence features

3.2.1. Turbulence intensity

The turbulence intensity is defined from the streamwise and cross-stream component of the fluctuating velocities (u and v), and expressed as follows:

$$TI = [(\overline{u^2} + \overline{v^2})/2]^{1/2}. \quad (6)$$

We have also reported previously the turbulence intensity profiles [11], and for the clarity of the present discussion, a portion of them is represented in this section. Figs. 5(a)–(b) show the center plane profiles of turbulence intensity at three measurement stations for each case of the injection location. The effects of increasing the specific momentum ratio of the injection to the turbulence intensity are more pronounced in case of the

near step injection, $l_f/H = 2$ (Fig. 5(a)) compared to the near reattachment zone injection, $l_f/H = 4$ (Fig. 5(b)). The profiles show two regions with different tendency in responding to the increase in injection momentum. Near the base wall, the turbulence intensity is suppressed by increasing the injection momentum, while in the shear layer region, the turbulence becomes stronger.

The spanwise distribution of turbulence intensity at three different heights above the injection point for the two cases of injection location is shown in Figs. 5(c) and (d). As in the profiles of mean streamwise velocity previously discussed, the increase of specific momentum ratio of the injection tends to enhance the uniformity of the turbulence intensity profile along the spanwise direction, until the region where the wall effect becomes prominent. Another interesting matter to note is that in every case of injection location, when approaching the sidewall region, the turbulence intensity at free stream increases, at the shear layer region decreases and at the recirculation zone maintains its center plane value. Hence, very near to the sidewall, the turbulence intensity seems to converge to a certain "wall value" regardless of the vertical position or the specific momentum ratio of injection. However, comparing the wall value of the turbulence intensity in Figs. 5(c) and (d), one can see that it increases as the streamwise position increases. At $x/H = 2$, it is about 10% of the mean freestream velocity, meanwhile at $x/H = 4$, it increases to about 16% of the freestream value. This is an indication that the turbulent boundary layer is formed over the sidewall and it is a function of the streamwise position with less influence from the main flow.

Figs. 5(a) and (b) also include the plot of ratio between the root mean square (rms) of the cross-stream and the streamwise fluctuating velocity ($\sqrt{\overline{v^2}}/\sqrt{\overline{u^2}}$). It is considered worthwhile to discuss this to help elucidating the detail of each component role in the turbulence structure of the flow field as well as to provide references for numerical works. In the case of $l_f/H = 2$, the rms ratio in the freestream center region maintains value less than unity of about 0.87, and it is apparently not influenced by the specific momentum ratio of injection. The ratio increases monotonically while entering the shear layer region and it reaches a value of about unity around the center of shear layer region. Considering that the turbulence intensities in this region reach the maximum value, it is understood that in this region, the streamwise and the cross-stream velocity fluctuations are the highest. In the recirculation zone, except for the case of the highest I, the rms ratio decreases when approaching the base wall. In this zone, increasing the specific momentum ratio of the injection, increases the rms ratio. However, from the facts that the turbulence intensity in the near base wall region decreases as the specific momentum of injection increases, it can be figured out that the augmentation of cross-stream fluctuation occurs simultaneously with the suppression of streamwise one with the former being less in the degree than the later. On the other hand, in the case of $l_f/H = 4$, along the vertical position, the rms ratio shows a rather constant value centered at about 0.85–0.9 with a weak tendency that the rms ratio increases as the specific momentum ratio of injection increases. This indicates that the contribution of streamwise and cross-stream fluctuation to the total turbulence intensity is in the same order.

3.2.2. Shear stress

Some important characteristics of the Reynolds shear stress are shown in Fig. 6. To ensure that the measurement is reliable enough to yield valid data, the result in the case of no injection is first examined against the available reference data. In this matter, the well-recognized envelope of acceptable data of maximum Reynolds shear stress suggested by Eaton and Johnston [1] is used, and is indicated in Fig. 6. The maximum Reynolds shear stress data for no injection case of the present measurements fall inside the suggested envelope. Thus, the deviation of Reynolds shear stress beyond the envelope is considered solely as the effect of the gas injection not because of any problem encountered in the measurement. In the case of $l_f/H = 2$ in Fig. 6(a), within the shear layer region, the level of Reynolds shear stress is high due to the steep velocity gradient and high-velocity fluctuation. When the injection momentum is increased, the Reynolds shear stress becomes higher and the maximum value goes beyond the envelope. Meanwhile, in the lower side of the recirculation zone, a slight change of the Reynolds stress can be observed at the location of injection and its upstream, with a tendency that the value decreases. Negative values of Reynolds shear stress are observed in this region in case of the injection with a high-specific momentum ratio ($I = 0.1$ and 0.3). These negative values are consistent with the mean profiles of the streamwise velocity, which have negative gradient ($\partial U/\partial y < 0$) in the region. This further indicates that in the case of high-specific momentum ratio, the upstream region from the injection point is dominated by a jet-like flow structure so that the shear stresses are negative [16]. Meanwhile, Fig. 6(b) shows a qualitatively similar behavior of the Reynolds shear stress except that no negative value of Reynolds shear stress can be observed. Although quantitatively, the degree of change is less than the near step injection case, in the shear layer, the Reynolds shear stress also increases as the injection momentum is increased. Shear stress also decreases in the region near the wall, however it is limited to the upstream and near the injection point.

The distribution of Reynolds stress along the spanwise positions of three different heights is shown in Figs. 6(c) and (d). The Reynolds shear stress shows a similar trend to that of turbulence intensity when approaching

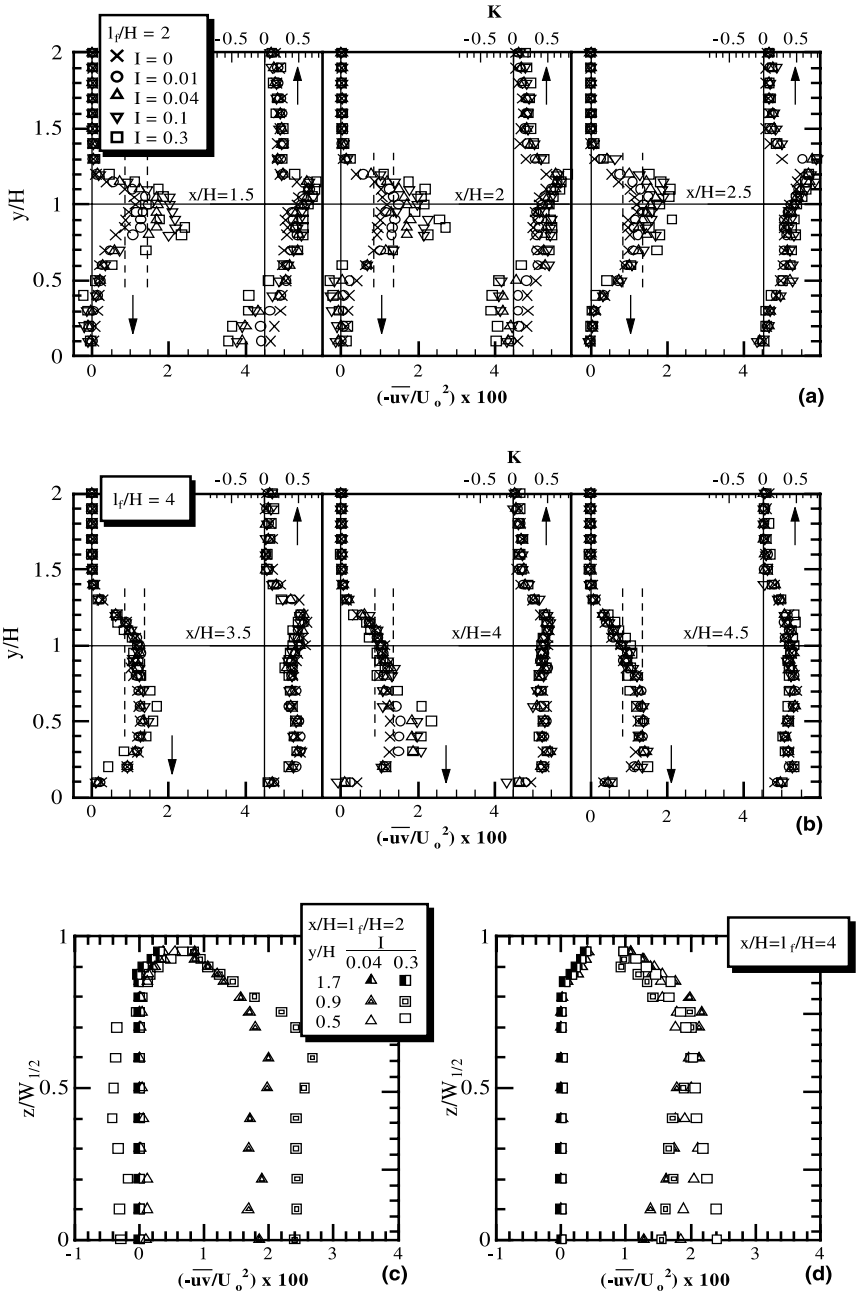

Fig. 6. Profiles of Reynolds shear stress and shear correlation. Center plane distribution in case of: (a) $l_f/H = 2$; (b) $l_f/H = 4$, and spanwise distribution above the injection in case of (c) $l_f/H = 2$; (d) $l_f/H = 4$.

the wall region. In this case, for $l_f/H = 2$, all the profiles approach a value of $0.007U_o^2$ regardless of the vertical position or the specific momentum of injection. For $l_f/H = 4$, although it is not as remarkable as the previous one, the Reynolds shear stresses approach a higher value of about $0.009\ U_o^2$. The agreement between the Reynolds shear stress and the turbulence intensity characterized the near wall region indicating that the side wall boundary has its own turbulence structure regardless the vertical position, the flow condition in the corresponding spanwise position adjacent to the wall region, and the specific momentum ratio of injection. However, it is a function of streamwise position from the step.

In Figs. 6(a) and (b), the profiles of the shear correlation coefficient ($K = -\overline{uv}/(\sqrt{\overline{u^2}}\sqrt{\overline{v^2}})$) are also plotted. They show the characteristics of the shear layer development. In case of $l_f/H = 2$ at Fig. 6(a), for every case of specific momentum ratio of injection, the profile has a peak value, which is clearly observed. If one takes arbitrarily the outer boundary of shear layer to correspond to position where the shear correlation coefficient reaches $K = 0.5$ as it increases from the freestream value, the peak value lies closely to this boundary. In the shear layer region, increasing the specific momentum ratio of the injection tend to increase the correlation coefficient. However, this trend is less remarkable in the measurement stations downstream the injection point. In the recirculation zone at $x/H = 1 \sim 2$, the profiles show negative values of correlation, mostly in the case of injection with specific momentum ratio greater than 0.04, which is primarily attributed to negative shear stress. Meanwhile in Fig. 6(b) for the case of $l_f/H = 4$, within the shear region, the correlation coefficient profiles display more flat appearances with K approximately constant and equal to about 0.5, but near the base wall, the correlation decreases. Effect of the injection to the correlation is not remarkable, as the profiles tend to collapse into single curve for every case.

3.3. Coherent structure properties

Assessment of the coherent structure properties is done directly on the tomographic image. Fig. 7 represents an example of a time-series image, and the terminology used in the measurement of the structure. To determine the convection velocity and the growth of the structure, the distance and the size of individual structure were tracked starting from the initial position it was induced for several consecutive time intervals as shown in Fig. 7.

3.3.1. Convection velocity

The characteristic of mean convection velocity of the coherent structure under the influence of gas injection is shown in Fig. 8, for the two cases of injection location. For each specific momentum ratio of injection, the mean convection velocity is calculated as the mean of the difference between two consecutive positions per unit time ($\overline{U_{cv}} = (\overline{dx_{cs}/dt})$). The virtual origins of the two plots in Fig. 8 converge to about 0.52 U_o, which indicates the convection velocity of the structure under no influence of gas injection. This is little bit different from the result of Reulet et al. [17] who reported a value of about 0.64 U_o for the same mean freestream velocity of the present study. However, it is quite in agreement with the suggestion of Brown and Roshko [18] that the coherent structures generated by the velocity gradient inside the shear layer behave as if they were in a mixing layer and convected by a mean movement with velocity about 50% of freestream velocity. Furthermore, it is obvious that the effect of gas injection is significant only in the case of near step injection. As the specific momentum ratio of injection is increased in case of $l_f/H = 2$, the convection velocity of the coherent structure decreases. At the highest specific momentum ratio in the present study, it decreases up to 10% compared to the case of no injection. We considered that the suppression of the convection velocity stems for a couple of mechanisms. The increase of injection momentum, which also means the increase of mass bleed, supports more mass entrainment from the recirculation zone into the mixing layer. Therefore, the mass content of the coherent structures will increase, and as a consequence of momentum conservation which is retained by those moving structures, their bulk convection velocity will decrease. Recalling the attenuation of vorticity in the mixing layer region due to the increase of injection momentum in Section 3.1.3 (Fig. 4), the rationale behind this could be similar in sense that the swirling structures also maintain their angular momentum conservation. Another influencing mechanism we conjectured is that the hydrodynamics disturbance caused by the injected jet flow to the mixing layer condition which restrict the structures movement that may be responsible for the suppression of the convection velocity. On the other hand, in case of injection at $l_f/H = 4$, the convection velocity tends to be constant regardless the ratio of specific momentum of injection. It is suggesting that the mechanisms proposed above do not take place in case of the injection of the gas near the reattachment due to the domination of high-shear turbulent flow over the injected gas flow in that region.

3.3.2. Scale growth

Fig. 9(a) shows the mean-scale growth rate of the moving structure measured as the change of the height of the structure in a unit time ($\overline{dh_{cs}/dt}$). In Fig. 9(a), the mean height of the first swirling structure ($\overline{h_{cs,1}}$) is also indicated. The growth rate of the size of the coherent structure is apparently not influenced by the gas injection, as the values do not vary significantly and are concentrated at about 1.5–1.55 mm/ms, regardless the ratio of the specific momentum as well as the location of the injection. However, in case of the injection at near step location, $l_f/H = 2$, the initial size of the structure is remarkably influenced by the injection of the gas, as the height of the swirling structure decreases when the specific momentum ratio of injection is increased. This suggests that the coherent structures with smaller size of swirling structures can be expected when the gas is injected with higher specific momentum ratio at the near step location. This can be confirmed by Fig. 9(b) which shows the comparison of spatial evolution of the coherent structures between the case of $I = 0.04$ and 0.3. However, we have considered that the mass content in

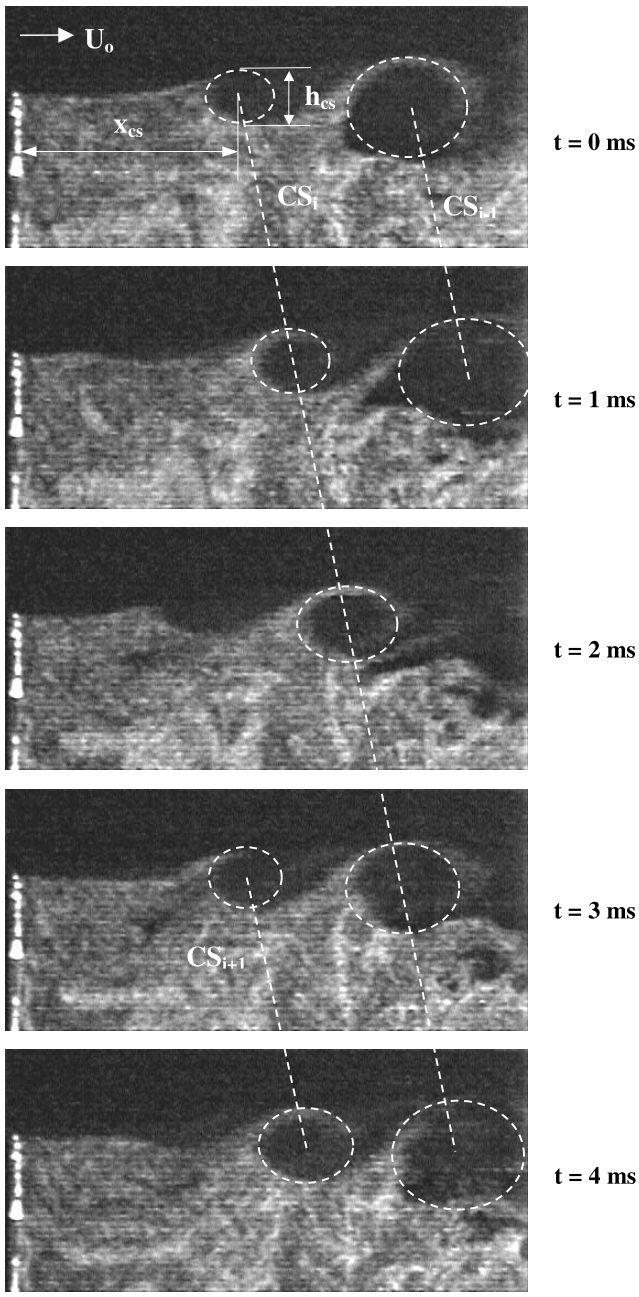

Fig. 7. Examples of time-series image showing the coherent structures evolution and the terminology of the measurement ($l_f/H = 4$, $I = 0.3$).

the coherent structure increases due to more mass entrainment with the increase of specific ratio of injection momentum. Therefore, the decrease of the size of the structure should be associated with the increase of the mass concentration within the structure. Qualitative observation of the brightness and quantitative value of luminosity of the processed image have confirmed this. The decrease of coherent structure size might be another indication of the effect of hydrodynamic disturbance exposed to the mixing layer by the gas jet injection flow.

3.3.3. Detachment of the structure

Detaching phenomenon of the coherent structure was examined from the luminosity spectra of the image

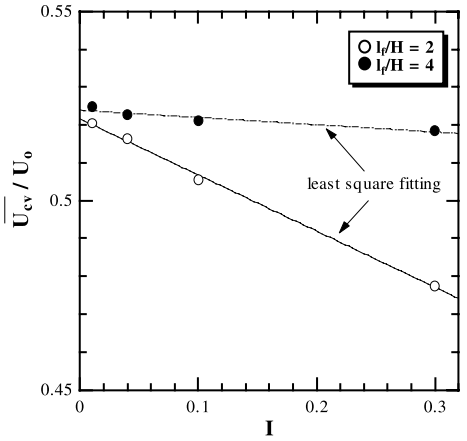

Fig. 8. Effects of the gas injection to the convection velocity of the coherent structures.

taken in the vicinity of the detachment location defined as the mean horizontal location where the first swirling structure induced ($\overline{x_{cs,1}}$). Typical time-series data of luminosity and the obtained spectrum from fast Fourier transforming the data are shown in Fig. 10(a) for the case of $l_f/H = 2$ and $I = 0.04$. The spectrum shows clearly a single peak whose frequency corresponds to the frequency of the swirling structure detachment. In Fig. 10(b), the effect of various specific momentum ratio of gas injection to the detaching frequency (f_{dc}) and the detachment location ($\overline{x_{cs,1}}$) are summarized. The virtual origin of the plot that represents the case of no injection shows that the detachment initially occurs around 0.9 step height from the step edge with frequency of detachment about 368 Hz. These values are rather different to the observation of Reulet et al. [17], who found mean detachment location of 0.75 step height and frequency about 240 Hz. When the gas is injected near the step, $l_f/H = 2$, the detachment frequency is obviously influenced by the variation of injection. The detachment frequency decreases as the specific momentum ratio is increased. The decrease of frequency reaches about 10% in case of the highest specific momentum ratio in the experiment ($I = 0.3$) compared to the case of no injection. Furthermore, it is understood that the detachment takes place closer to the step edge by increasing the specific ratio of injection momentum. These results suggest that the gas injection apparently suppresses the detachment of the coherent structure, and this effect becomes stronger as the specific momentum ratio is increased. The rationale behind this is probably a combination of the increase of the hydrodynamic disturbance of the injected jet flow and the alteration of turbulence structures (turbulence intensity and Reynolds shear stress increase) in the vicinity of detachment which support a damping effect to the shear instability. On the other hand, when the gas is injected at $l_f/H = 4$, neither the detachment frequency nor the detachment location is influenced by the variation of gas injection, as their values do not remarkably vary, but constant to the virtual value of no injection case. This again confirms that due to the domination of higher flow velocity and shear turbulence near reattachment region as well as some distance apart from the step edge where the initial stage of coherent structure is induced, the gas injection in this location does not give prominent influence to the coherent structure characteristics.

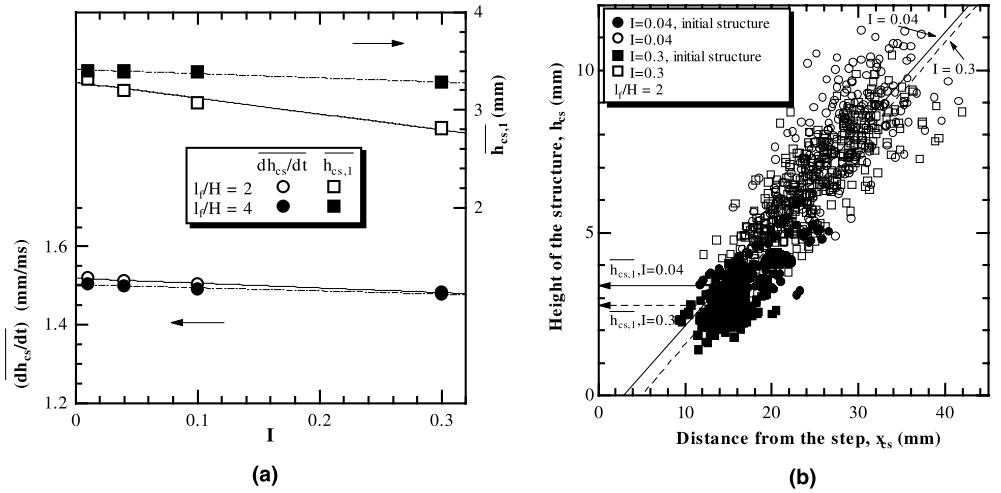

Fig. 9. Growth of the coherent structures: (a) effect of gas injection to the temporal scale growth and mean height of initial structure; (b) comparison of spatial evolution of the coherent structure for $l_f/H = 2$, $I = 0.04$ and 0.3.

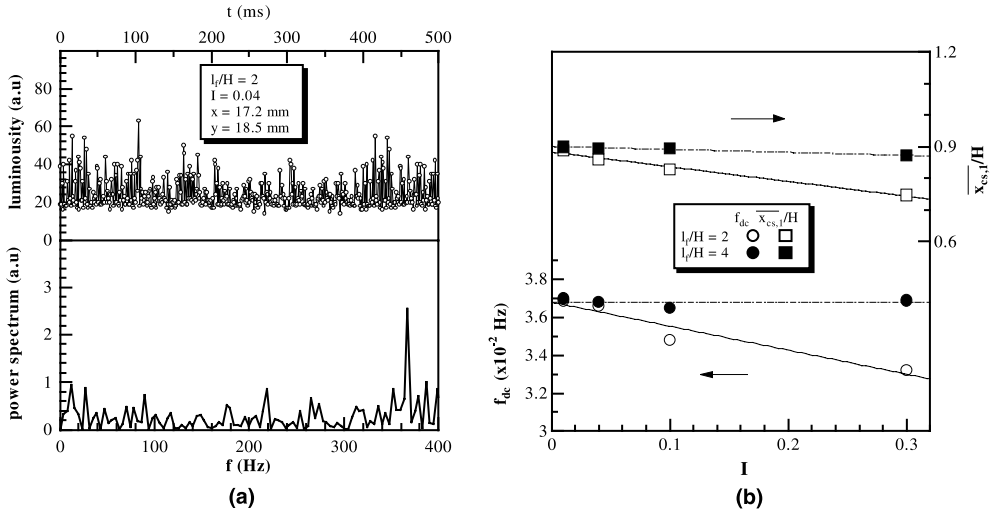

Fig. 10. Detaching phenomenon of the coherent structure: (a) typical time-series data and power spectrum of luminosity at mean location of detachment; (b) effects of gas injection to detaching frequency and mean location of detachment.

4. Summary and concluding remarks

We have experimentally studied the effect of a gas injection from a slot port to the turbulent velocity field of a subsonic backward facing step flow and to the characteristics of the coherent structure. Two main parameters, the specific momentum ratio and the location of injections have been varied and their effects have been discussed with the focus on the flow field in the recirculation zone and the shear layer region. The summary and conclusions are:

(1) More remarkable effect of the gas injection to the examined quantities (mean flow, turbulence properties, coherent structure characteristics) occurred mostly in case of injection near the step ($l_f/H = 2$) compared to the injection near the reattachment region ($l_f/H = 4$).

(2) In the case of gas injection near the step location, it is found that the mean flow field is characterized by the splitting of the recirculation zone into two parts, upstream and downstream of the injection point, and the creation of a region in the upstream of injection point having mean vorticity in the opposite direction to that initially exists there when no injection be imposed. When the specific momentum ratio of injection is increased, the convective mass transfer is more supported toward the upstream recirculation zone due to the less flow restriction in the region. For the case of the highest specific momentum ratio in the experiment ($I = 0.3$), the mean streamlines pattern ($\overline{\psi}/(U_o H)$) indicates that the increase of mass flow rate in the upstream recirculation zone is as much as four times to that in the downstream one. Moreover, from the spanwise distribution of mean velocity profiles, it is obvious that an increase of the specific momentum ratio of injection extents the two dimensionality of the flow field not less than 75% of the spanwise width of the flow field.

(3) Measurement of the turbulence quantities indicates that within the region not influenced by the sidewall boundary effect, as the injection momentum is increased, the turbulent intensity and the Reynolds shear stress increase in the shear layer region, while they tend to decrease in the reverse flow zone. The spanwise distributions show an agreement between the trends of the turbulence intensity and the Reynolds shears as they approach the sidewall. Then, both quantities characterized the near wall region with certain wall values which further suggest that the sidewall boundary has a distinctive turbulence structure regardless the vertical position, the flow condition in the corresponding spanwise position adjacent to the wall, and the momentum of injection, but a function of the streamwise position from the step.

(4) When the specific momentum ratio of injection near the step location is increased, the characteristics of coherent structure in the shear mixing layer are significantly altered, denoted by the decrease in the convection velocity, the spatial size of the structures along their paths, the frequency as well as the horizontal location of the detachment of not less than 10% for the case of highest specific momentum ratio compared to no injection case. When the specific momentum ratio of the injection is increased, more mass entrains into the mixing layer and makes the mass content in the coherent structure increase. Consequent to the linear and angular momentum conservations retained by the moving structure, the bulk convection velocity of the structure as well as the vorticity within the region decrease. Furthermore, the hydrodynamic disturbances from the jet

injection flow to the mixing layer and the alteration of turbulence characteristics which become more significant as the injection momentum increases contribute important roles to the suppression of the coherent structure properties.

(5) As an important result regarding the mixing process in the current flow configuration, it is revealed that some competing factors characterized it. While ensuring most mass fraction of the injected gas to mix with the recirculating air, the injection near the step location, especially with high momentum, imposes suppression to the coherent structuring in the shear layer, which may disfavor the local patterns of mixing. On the other hand, the gas injected near reattachment region mix well with the surrounding air due to the higher shear turbulence and it does not affect the coherent structures. However, as revealed by the streamlines pattern, with the increase of injection momentum, more fraction of the gas is unused, does not mix with the recirculating airflow, but carried away by the freestream. Thus, these results provide a basis and valuable information in developing an efficient design of a combustor from the viewpoint of enhancing the gas–air mixing process by attaining the balance of those competing factors, between the geometrical and fluid dynamical parameters of injection.

Acknowledgements

This work was supported by a grant from the Japanese Ministry of Education. The authors would like to thank M. Sakai and Y. Shimozono for helping the experimentation and the Hitachi Scholarships Fnd. for financial support to the first author to do the research in Japan.

References

[1] J.K. Eaton, J.P. Johnston, A review of research on subsonic turbulent flow reattachment, AIAA J. 19 (1981) 1093–1099.
[2] D.W. Etheridge, P.H. Kemp, Measurement of turbulent flow downstream of a rearward-facing step, J. Fluid Mech. 86 (3) (1978) 545–566.
[3] G. Papadopoulus, M.V. Otugen, Separating and reattaching flow structure in a suddenly expanding rectangular duct, Trans. ASME J. Fluid Eng. 117 (1995) 17–23.
[4] W.A. de Groot, R. Latham, J.I. Jagoda, W.C. Strahle, Rayleigh measurements of species concentration in a complex turbulent flow, AIAA J. 25 (8) (1985) 1142–1144.
[5] W.A. de Groot, R.E. Walterick, J.I. Jagoda, Combined LDV and Rayleigh measurement in a complex turbulent mixing flow, AIAA J. 27 (1) (1989) 108–110.
[6] J.T. Yang, B.B. Tsai, G.L. Tsai, Separated-reattaching flow flow over a backstep with uniform normal mass bleed, Trans. ASME J. Fluid Eng. 116 (1994) 29–35.
[7] J.T. Yang, C.H. Tsai, High temperature heat transfer of separated flow over as sudden expansion with base mass injection, Int. J. Heat Mass Transfer 39 (11) (1996) 2293–2301.
[8] Y.T. Yang, C.L. Kuo, Numerical study of a backward-facing step with uniform mass bleed, Int. J. Heat Mass Transfer 40 (7) (1997) 1677–1686.
[9] M. Haibel, F. Mayinger, The effect of turbulent structures on the development of mixing and combustion process in sub- and supersonic H_2 flames, Int. J. Heat Mass Transfer 37 (Suppl.1) (1994) 241–253.
[10] C.M. Coats, Coherent structures in combustion, Prog. Energy Combust. Sci. 22 (5) (1996) 427–509.
[11] Harinaldi, T. Ueda, A. Matsuo, M. Mizomoto, On the turbulence of a reattaching separated flow with the existence of gas injection, in: J.K. Eaton, S. Banerjee (Eds.), Turbulence and Shear Flow–1 First International Symposium, Beggel House, Inc, New York, 1999, pp. 939–944.
[12] T. Ueda, Y. Yahagi, M. Mizomoto, Mie scattering with silicon oil droplets in combustion field, Trans. Jpn. Soc. Mech. Eng. 57 (541,B) (1991) 3255–3259 (in Japanese).
[13] B.F. Armaly, F. Durst, J.C.F. Pereira, B. Schonung, Experimental and theoretical investigation of backward-facing step flow, J. Fluid Mech. 127 (1983) 473–496.
[14] P.T. Williams, A.J. Baker, Numerical simulations of laminar flow over a 3D backward-facing step, Int. J. Numer. Meth. Fluids 24 (1997) 1159–1183.
[15] T.P. Chiang, T.W.H. Sheu, A numerical revisit of backward-facing step flow problem, Phys. Fluids 11 (4) (1999) 862–874.
[16] T. Tatsumi, The Science of Turbulence Phenomena, Tokyo University Press, 1986, p. 377 (in Japanese: Ranryu Gensho no kagaku).
[17] P. Reulet, J. Dumoulin, P. Millan, Experimental investigation of a flow behind a backward-facing step by tomographic visualization, laser velocimetry and infrared thermography measurement, ASME-FED Exp. Numer. Flow Vis. 218 (1995) 171–180.
[18] G.L. Brown, A. Roshko, On the density effects and large structure in two-dimensional mixing layers, J. Fluid Mech. 64 (1974) 775–816.